

Article

Cyanide Complexes Based on $\{\text{Mo}_6\text{I}_8\}^{4+}$ and $\{\text{W}_6\text{I}_8\}^{4+}$ Cluster Cores

 Aleksei S. Pronin ¹, Spartak S. Yarovoy ¹, Yakov M. Gayfulin ^{1,*}, Aleksey A. Ryadun ¹, Konstantin A. Brylev ¹, Denis G. Samsonenko ¹, Ilia V. Eltsov ² and Yuri V. Mironov ^{1,*}

¹ Nikolaev Institute of Inorganic Chemistry SB RAS, 3, Acad. Lavrentiev ave., 630090 Novosibirsk, Russia; pronin@niic.nsc.ru (A.S.P.); YSS@niic.nsc.ru (S.S.Y.); ryadunalexey@mail.ru (A.A.R.); brylev@niic.nsc.ru (K.A.B.); denis@niic.nsc.ru (D.G.S.)

² Department of Natural Sciences, Novosibirsk State University, 2, Pirogova str., 630090 Novosibirsk, Russia; eiv@fen.nsu.ru

* Correspondence: gayfulin@niic.nsc.ru (Y.M.G.); yuri@niic.nsc.ru (Y.V.M.)

Academic Editor: Constantina Papatriantafyllopoulou

Received: 10 November 2020; Accepted: 4 December 2020; Published: 8 December 2020



Abstract: Compounds based on new cyanide cluster anions $[\{\text{Mo}_6\text{I}_8\}(\text{CN})_6]^{2-}$, $\text{trans}-[\{\text{Mo}_6\text{I}_8\}(\text{CN})_4(\text{MeO})_2]^{2-}$ and $\text{trans}-[\{\text{W}_6\text{I}_8\}(\text{CN})_2(\text{MeO})_4]^{2-}$ were synthesized using mechanochemical or solvothermal synthesis. The crystal and electronic structures as well as spectroscopic properties of the anions were investigated. It was found that the new compounds exhibit red luminescence upon excitation by UV light in the solid state and solutions, as other cluster complexes based on $\{\text{Mo}_6\text{I}_8\}^{4+}$ and $\{\text{W}_6\text{I}_8\}^{4+}$ cores do. The compounds can be recrystallized from aqueous methanol solutions; besides this, it was shown using NMR and UV-Vis spectroscopy that anions did not undergo hydrolysis in the solutions for a long time. These facts indicate that hydrolytic stabilization of $\{\text{Mo}_6\text{I}_8\}$ and $\{\text{W}_6\text{I}_8\}$ cluster cores can be achieved by coordination of cyanide ligands.

Keywords: cluster compounds; molybdenum; tungsten; cyanide ligand; crystal structure; luminescence; hydrolytic stability

1. Introduction

Chemistry and applications of compounds based on octahedral cluster cores $\{\text{M}_6\text{X}_8\}^{4+}$ ($\text{M} = \text{Mo}$ or W ; $\text{X} = \text{Cl}$, Br or I) have been studied for several decades due to a number of interesting physicochemical properties, including bright luminescence in the red and near infrared regions [1–7] and reversible redox transformations [8,9]. High luminescence quantum yields and lifetimes in combination with tunability of chemical properties by changing ligand environments made it possible to create a number of promising luminescent and photocatalytic materials based on these clusters [10–15]. The phosphorescence of clusters is also associated with the efficient singlet oxygen production [16,17]. Therefore, compounds and materials based on $\{\text{M}_6\text{X}_8\}^{4+}$ clusters can potentially be applied in photodynamic therapy [18–22], antibacterial and antiviral applications [23–25]. Besides this, luminescence of clusters was successfully used in bioimaging [18,26,27].

An interesting and less studied area is the use of luminescent octahedral cluster complexes of molybdenum and tungsten as building blocks for the synthesis of functional coordination polymers. High symmetry and large volume of the cluster complexes make them convenient for the design of crystalline coordination polymers and metal-organic frameworks, while the spectroscopic and redox features of the clusters can be used in order to impart the desired functionality to the solid material. The majority of coordination polymers based on octahedral metal cluster complexes known to date have been obtained based on the cyanide-coordinated clusters [28–30]. The presence of ambidentate apical cyanide ligands makes it possible to coordinate transition and post-transition metal cations and to obtain

crystalline coordination polymers by self-assembly. Using $\{M_6X_8\}$ -type cyanoclusters is interesting for obtaining new luminescent coordination polymers. For now, the structure of only one cyanide cluster based on an $\{Mo_6X_8\}^{4+}$ core has been described in the literature, namely $[\{Mo_6Br_8\}(CN)_6]^{2-}$ [31,32], while the tungsten cyanide clusters of that type are unknown. Therefore, further progress in this field requires the development of methods for the synthesis of cyanide molybdenum and tungsten halide clusters.

In this work, we report on the synthesis of the first cyanide cluster anions based on $\{Mo_6I_8\}^{4+}$ and $\{W_6I_8\}^{4+}$ cores, namely $[\{Mo_6I_8\}(CN)_6]^{2-}$, *trans*- $[\{Mo_6I_8\}(CN)_4(MeO)_2]^{2-}$ and *trans*- $[\{W_6I_8\}(CN)_2(MeO)_4]^{2-}$. Their crystal structures and spectroscopic properties in the solid state and solutions were investigated together with calculated geometry and electronic structures. To obtain new compounds, two different ways of synthesis were tested, namely, substitution of terminal iodide ligands in solvothermal conditions and mechanochemical depolymerization of Mo_6I_{12} . Each way was found to be usable for obtaining target compounds in preparative amounts. The new anions have shown an outstanding stability in aqueous solutions, demonstrating the stabilizing influence of terminal cyanides.

2. Results and Discussion

2.1. Synthesis

Until now, only one structure of a cyanide cluster based on halide octahedral molybdenum core has been reported, namely $[Mo_6Br_8(CN)_6]^{2-}$ [31]. It was shown that this complex formed polymeric compounds with transition metal cations [32]. For octahedral tungsten halides, cyanide compounds have not been described. At the same time, complexes based on $\{Mo_6I_8\}^{4+}$ and $\{W_6I_8\}^{4+}$ cluster cores are usually very bright luminophores, which makes them interesting as components of supramolecular systems and coordination polymers.

In this work, two approaches were realized for the preparation of cyanide cluster complexes based on $\{Mo_6I_8\}^{4+}$ and $\{W_6I_8\}^{4+}$ cores (Scheme 1). The first approach is depolymerization of M_6I_{12} compounds by mechanochemical activation. The reaction between polymeric Mo_6I_{12} and NaCN in the ball mill led to the formation of water-soluble products. After filtration of the solution, addition of CsCl and evaporation, an orange microcrystalline powder was isolated, which was identified as $Cs_{1.3}Na_{0.7}[\{Mo_6I_8\}(CN)_6] \cdot 2H_2O$ (1) based on elemental analysis and EDS. The reaction of an aqueous solution of this compound with an aqueous solution of Bu_4NI led to the precipitation of the compound $(Bu_4N)_2[\{Mo_6I_8\}(CN)_6] \cdot 0.7H_2O$ (2), which is soluble in polar organic solvents and can be easily recrystallized from CH_3CN/H_2O or $MeOH/H_2O$ mixtures. Recrystallization from dimethyl sulfoxide (DMSO) led to removal of the solvate H_2O molecules and precipitation of compound 3. The yield of compound 2 is about 50% with respect to the initially taken Mo_6I_{12} , which makes it possible to obtain it in preparative amounts. It was also shown that this compound can be obtained with a very low yield in a solvothermal reaction between the salt $(Bu_4N)_2[\{Mo_6I_8\}I_6]$ and NaCN in an aqueous solution. The reaction gave an insoluble brown precipitate and a cloudy yellow solution, from which, after filtration and evaporation, several crystals of compound 2 were isolated. An attempt to obtain a tungsten analog of the $[\{Mo_6I_8\}(CN)_6]^{2-}$ anion by mechanochemical activation of W_6I_{12} in the presence of NaCN was unsuccessful: the resulting brown-black product was unstable to hydrolysis. It is interesting to note that soluble trinuclear clusters of both molybdenum and tungsten, namely $(Et_4N)_2[W_3S_7Br_6]$, $(Et_4N)_2[W_3Se_7Br_6]$, and $[Mo_3Se_7(dtc)_3]dte$ ($dte = diethyldithiocarbamate$), were synthesized earlier using mechanochemical activation of polymeric solids $W_3S_7Br_4$, $W_3Se_7Br_4$ and $Mo_3Se_7Br_4$, respectively [33].

samples match those for the freshly prepared compounds. Octahedral halide cluster complexes of molybdenum and tungsten usually have low hydrolytic stability because of replacement of the apical ligands by H_2O or OH^- over time or hydrolysis of the cluster core itself [39]. Thus, the coordination of cyanide ligands significantly increased the hydrolytic stability of the clusters, which may open the way for investigation of their potential biological applications.

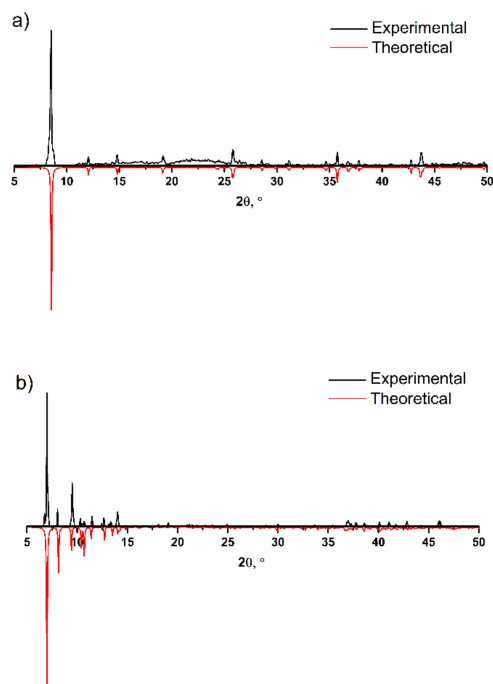


Figure 1. Experimental (top) vs calculated (bottom) powder diffraction patterns for compounds **4** (a) and **5** (b).

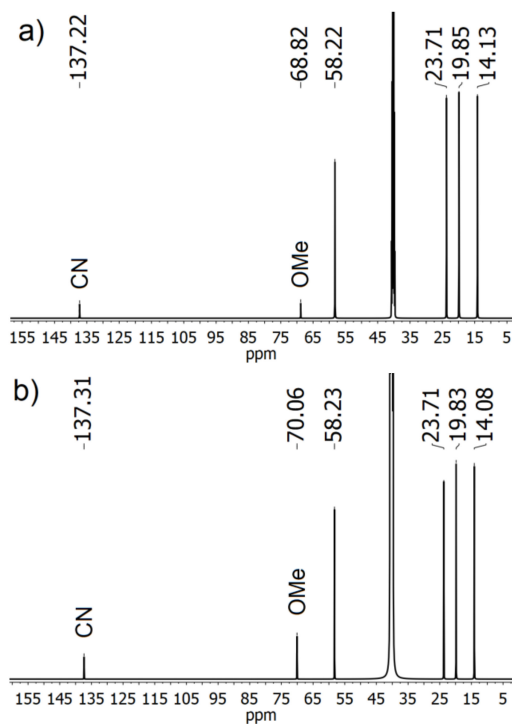
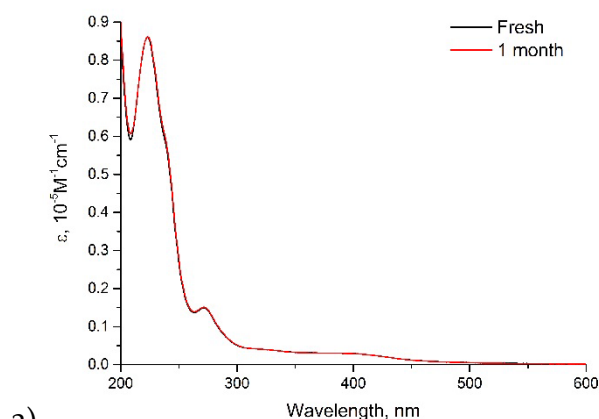
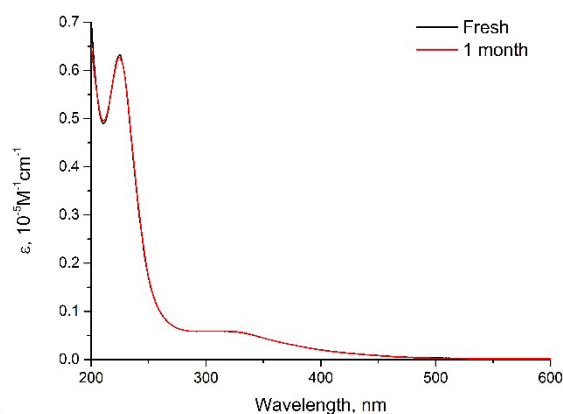


Figure 2. Experimental ^{13}C -NMR spectra for compounds **4** (a) and **5** (b) in DMSO-d_6 solution.



a)



b)

Figure 3. UV-Vis spectra of compounds **4** (a) and **5** (b) recorded for the freshly prepared aqueous solutions and for the solutions aged for 1 month.

2.3. Crystal Structures

Compound $(\text{Bu}_4\text{N})_2[\{\text{Mo}_6\text{I}_8\}(\text{CN})_6]\cdot 0.7\text{H}_2\text{O}$ (**2**) crystallizes in monoclinic crystal system, $C2/c$ space group. Asymmetric unit contains two $[\{\text{Mo}_6\text{I}_8\}(\text{CN})_6]^{2-}$ cluster anions as well as four Bu_4N^+ cations with partially disordered CH_3 - groups and three partially occupied positions of solvate H_2O molecules. The $[\{\text{Mo}_6\text{I}_8\}(\text{CN})_6]^{2-}$ anion demonstrates a typical geometry of octahedral $\{\text{Mo}_6(\mu_3\text{-X}_8)\}$ ($\text{X} = \text{halide}$) cluster core containing 24 cluster valence electrons (Figure 4a, Table 1). The average Mo-Mo and Mo-I bond distances (2.680(5) and 2.773(8) Å, respectively) agree well with the corresponding values observed for clusters with $\{\text{Mo}_6\text{I}_8\}^{4+}$ core [40–42]. Each Mo atom of the cluster core is coordinated by apical CN^- ligand. The Mo-C distances display the average length of 2.188(8) Å, which is in the range of values that were reported for hexanuclear cyanide clusters of Mo [32,43,44]. The crystal packing includes the cluster anions forming a column along the a axis and Bu_4N^+ cations, which fill the space between anions forming a cationic sublattice with channel cavities (Figure 4b). The crystallographically observable lattice H_2O molecules are located in proximity with cluster anions forming hydrogen bonds (2.96–3.07 Å) with N atoms of CN^- ligands.

Compound $(\text{Bu}_4\text{N})_2[\{\text{Mo}_6\text{I}_8\}(\text{CN})_6]\cdot 2\text{DMSO}$ (**3**) crystallizes in the triclinic crystal system, $\bar{P}1$ space group. Asymmetric unit contains half of the cluster anions (three Mo atoms, four I atoms and atoms of three CN^- groups) as well as one Bu_4N^+ cation and one DMSO molecule (Figure S1). All positions are fully occupied. The structure of the cluster anion is similar to the one found in structure **2**. The crystal packing (Figure S2) is formed by the numerous interactions of hydrogen bond acceptors (O atoms of DMSO molecules and N atoms of CN^- groups) with $-\text{CH}_2-$ and CH_3- groups of Bu_4N^+ cations and DMSO molecules. The corresponding $-\text{CH}\cdots\text{O}$ and $-\text{CH}\cdots\text{N}$ distances are within the range of 3.26–3.60 Å. In addition, weak hydrogen bonds were observed between $-\text{CH}_3$ and $-\text{CH}_2-$ groups of

Bu_4N^+ cation and μ_3 -I ligands of cluster anions. The C-I distances are 3.88 and 3.77 Å for $-\text{CH}_3$ and $-\text{CH}_2$ - groups, respectively.

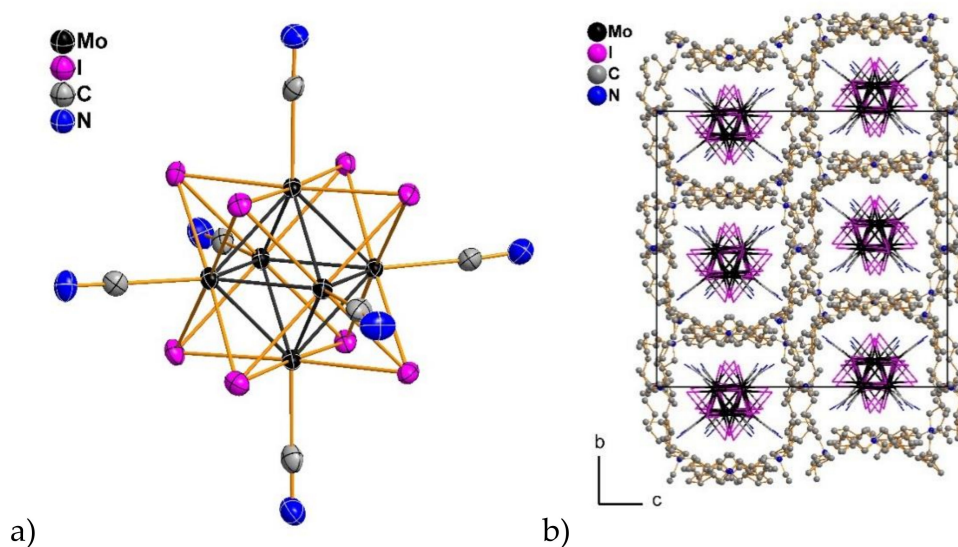


Figure 4. Structure of the $[\text{Mo}_6\text{I}_8(\text{CN})_6]^{2-}$ cluster anion in the structure of compound 2. Atoms are shown as thermal ellipsoids of 50% probability (a); packing of the cluster anions and Bu_4N^+ cations in the structure of compound 2, view in bc plane (b).

Table 1. Selected interatomic distances within $[\text{Mo}_6\text{I}_8(\text{CN})_6]^{2-}$, $\text{trans}-[\text{Mo}_6\text{I}_8(\text{CN})_4(\text{MeO})_2]^{2-}$ and $\text{trans}-[\text{W}_6\text{I}_8(\text{CN})_2(\text{MeO})_4]^{2-}$ clusters (range/average, Å) in the structures of compounds 2–5.

	$(\text{Bu}_4\text{N})_2[\text{Mo}_6\text{I}_8(\text{CN})_6]\cdot\text{H}_2\text{O}$ (2)	$(\text{Bu}_4\text{N})_2[\text{Mo}_6\text{I}_8(\text{CN})_6]\cdot 2\text{DMSO}$ (3)	$(\text{Bu}_4\text{N})_2[\text{Mo}_6\text{I}_8(\text{CN})_4(\text{MeO})_2]$ (4)	$(\text{Bu}_4\text{N})_2[\text{W}_6\text{I}_8(\text{MeO})_4(\text{CN})_2]\cdot 5\text{H}_2\text{O}$ (5)
M–M	2.6738(8)– 2.6904(8)/2.680(5)	2.6832(4)– 2.6990(3)/2.689(6)	2.6799(7)–2.6829(8)/2.681(1)	2.6558(4)– 2.6772(4)/2.6703(8)
M–I	2.7581(8)– 2.7903(7)/2.773(8)	2.7679(4)– 2.7907(3)/2.778(6)	2.7714(3)–2.7974(3)/2.78(1)	2.7998(5)–2.8388(5)/2.82(1)
M–C	2.177(8)– 2.200(8)/2.188(8)	2.19(3)3– 2.201(3)/2.196(4)	2.190(7)	2.195(7)
M–O	–	–	2.049(8)	2.049(5)–2.051(5)/2.050(1)

Compound $(\text{Bu}_4\text{N})_2[\{\text{Mo}_6\text{I}_8(\text{CN})_4(\text{MeO})_2\}]$ (4) crystallizes in tetragonal crystal system, $I4/mmm$ space group. Asymmetric unit contains two Mo atoms, one iodine atom, one CN^- group, one MeO^- group, and one N atom, four C atoms and 9 H atoms of Bu_4N^+ cation. Terminal $-\text{CH}_3$ group of Bu_4N^+ cation is disordered over two equivalent positions. Terminal $-\text{CH}_3$ group of MeO^- ligand is disordered over four positions by the 4-fold axis passing through the Mo and O atoms. All other positions are fully occupied. The $\text{trans}-[\{\text{Mo}_6\text{I}_8(\text{CN})_4(\text{MeO})_2\}]^{2-}$ cluster anion (Figure 5a) displays the $\{\text{Mo}_6\text{I}_8\}^{4+}$ cluster core, which is coordinated by four CN^- groups in the equatorial plane and two MeO^- groups in the trans -position. The corresponding Mo–C interatomic distances are 2.190(7) Å, and the Mo–O bonds are 2.049(8) Å. While the Mo–C distances match well the corresponding bond lengths found in other hexanuclear cyanide clusters of Mo, the Mo–O bonds are slightly shorter than ones reported previously for $[\text{Mo}_6\text{I}_8(\text{MeO})_6]^{2-}$ anion (2.055–2.110 Å) [3]. In comparison with structure 2, compound 4 demonstrates the different ways of packing cluster anions and Bu_4N^+ cations (Figure S3). Cluster anions are isolated in the center of pseudo-cubic cell formed by the alkyl groups of Bu_4N^+ cations.

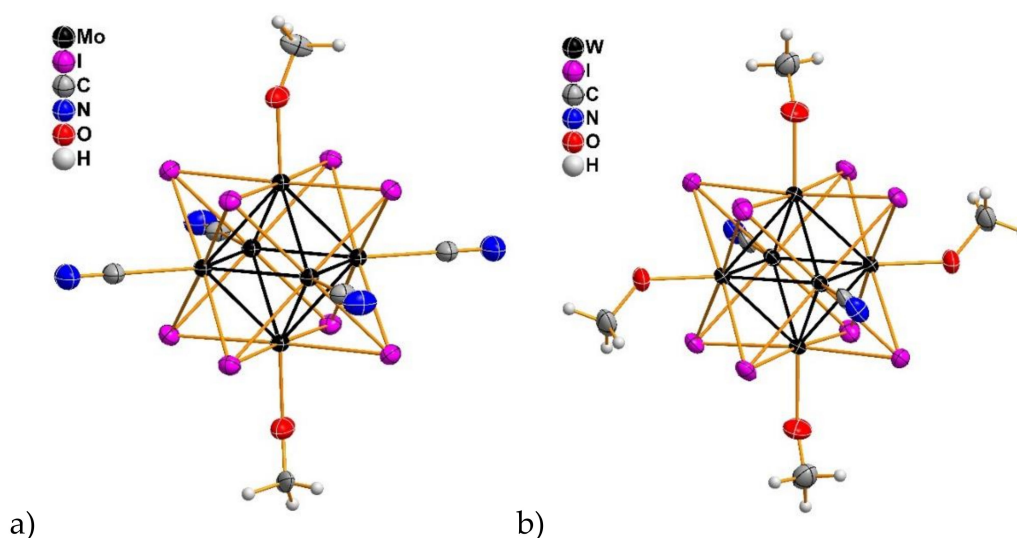


Figure 5. Structure of the $[\{\text{Mo}_6\text{I}_8\}(\text{CN})_4(\text{MeO})_2]^{2-}$ cluster anions in the structure of compound **4** (a); structure of the $[\{\text{W}_6\text{I}_8\}(\text{CN})_2(\text{MeO})_4]^{2-}$ cluster anion in the structure of compound **5** (b); atoms are shown as thermal ellipsoids of 50% probability.

Compound $(\text{Bu}_4\text{N})_2[\{\text{W}_6\text{I}_8\}(\text{MeO})_4(\text{CN})_2] \cdot 5\text{H}_2\text{O}$ (**5**) crystallizes in a monoclinic crystal system, $P2_1/n$ space group. The asymmetric unit includes half of the *trans*- $[\{\text{W}_6\text{I}_8\}(\text{CN})_2(\text{MeO})_4]^{2-}$ cluster anion (three W atoms, four I atoms, atoms of CN^- group, and two MeO^- ligands), one fully ordered Bu_4N^+ cation and four positions of O atoms of solvate H_2O molecules, three of which are partially occupied. The cluster anion represent the 24-electron $\{\text{W}_6\text{I}_8\}^{4+}$ core with a slightly distorted $\{\text{W}_6\}$ octahedron. The average W-W and W-I distances (2.671(8) and 2.82(1) Å, respectively) are comparable with the corresponding values found in hexanuclear tungsten iodides with various terminal ligands [1,2,34,45–47]. Two W atoms in the *trans*-position are coordinated by CN^- ligands, while four remaining W atoms in the equatorial plane are coordinated by a metholate anion (Figure 5b). The corresponding W-C and W-O distances are 2.195(7) and 2.048(5) Å, respectively. These bond lengths are similar to Mo-C bond lengths in the $[\{\text{Mo}_6\text{I}_8\}(\text{CN})_6]^{2-}$ cluster anion (Table 1) and Mo-O bond lengths in the $[\{\text{Mo}_6\text{I}_8\}(\text{MeO})_6]^{2-}$ anion.

The crystal packing of compound **5** (Figure S4) is formed by the cluster anions bound with solvate H_2O molecules by a net of hydrogen bonds. Particularly, terminal N atoms of CN^- groups form $\text{OH} \cdots \text{N}$ bonds with a length of 3.0 Å, while the O atoms of MeO^- ligands form $\text{OH} \cdots \text{O}$ bonds with a length of 2.82–2.87 Å. Lengths of $\text{OH} \cdots \text{O}$ bonds between H_2O molecules vary in the range of 2.80–2.99 Å. The Bu_4N^+ cations are included in the hydrogen-bonded framework of cluster anions and H_2O molecules.

2.4. Calculated Geometry and Electronic Structure

Optimized interatomic distances for $[\{\text{Mo}_6\text{I}_8\}(\text{CN})_6]^{2-}$, *trans*- $[\{\text{Mo}_6\text{I}_8\}(\text{CN})_4(\text{MeO})_2]^{2-}$ and *trans*- $[\{\text{W}_6\text{I}_8\}(\text{CN})_2(\text{MeO})_4]^{2-}$ cluster anions are close to the experimentally found values, although all calculated bond lengths tend to slightly increase (Table 2). Energy level diagrams in the near frontier region (Figure 6) show some differences between electronic structures of heteroligand clusters and $[\{\text{Mo}_6\text{I}_8\}(\text{CN})_6]^{2-}$ anions. Frontier orbitals of the latter include almost degenerated HOMO and HOMO-1, which are localized primarily on the $\{\text{Mo}_6\text{I}_8\}^{4+}$ core with a small contribution (~3%) of atomic orbitals of C and N atoms. In combination with cluster core-centered LUMO, electronic structure of this anion is typical for face-capped clusters of the $[\{\text{M}_6\text{X}_8\}\text{L}_6]$ type [48–51]. At the same time, HOMOs of *trans*- $[\{\text{Mo}_6\text{I}_8\}(\text{CN})_4(\text{MeO})_2]^{2-}$ and *trans*- $[\{\text{W}_6\text{I}_8\}(\text{CN})_2(\text{MeO})_4]^{2-}$ clusters include *p* orbitals of O and C atoms of terminal MeO^- ligands with the total contribution of about 10% for Mo

cluster and 7% for the W cluster. HOMO-LUMO gaps are 3.67, 3.33, and 3.43 eV for $[\{\text{Mo}_6\text{I}_8\}(\text{CN})_6]^{2-}$, $\text{trans}-[\{\text{Mo}_6\text{I}_8\}(\text{CN})_4(\text{MeO})_2]^{2-}$, and $\text{trans}-[\{\text{W}_6\text{I}_8\}(\text{CN})_2(\text{MeO})_4]^{2-}$ clusters, respectively.

Table 2. Calculated interatomic distances within $[\{\text{Mo}_6\text{I}_8\}(\text{CN})_6]^{2-}$, $\text{trans}-[\{\text{Mo}_6\text{I}_8\}(\text{CN})_4(\text{MeO})_2]^{2-}$ and $\text{trans}-[\{\text{W}_6\text{I}_8\}(\text{CN})_2(\text{MeO})_4]^{2-}$ clusters (range/average, Å).

	$[\{\text{Mo}_6\text{I}_8\}(\text{CN})_6]^{2-}$	$[\{\text{Mo}_6\text{I}_8\}(\text{CN})_4(\text{MeO})_2]^{2-}$	$[\{\text{W}_6\text{I}_8\}(\text{CN})_2(\text{MeO})_4]^{2-}$
M–M	2.711	2.704–2.722/2.712(8)	2.692–2.707/2.699(4)
M–I	2.862	2.872–2.934/2.89(2)	2.912–2.992/2.95(3)
M–C	2.207	2.218	2.214
M–O	–	2.018	2.020

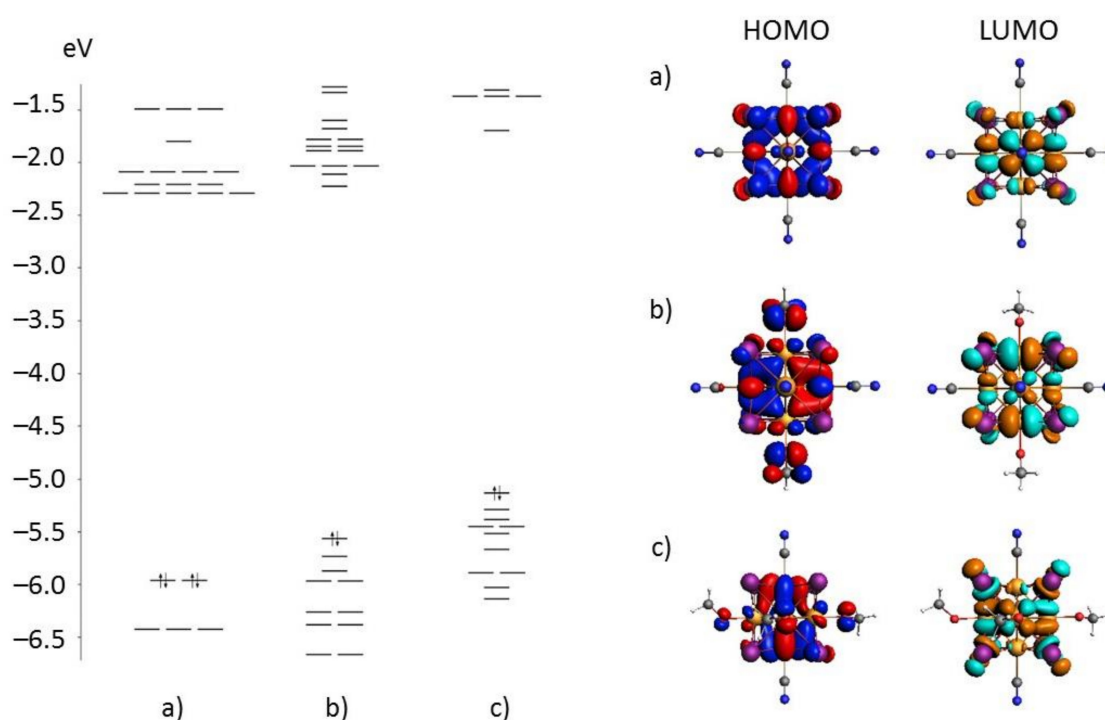


Figure 6. Left: energy level diagrams of the $[\{\text{Mo}_6\text{I}_8\}(\text{CN})_6]^{2-}$, $\text{trans}-[\{\text{Mo}_6\text{I}_8\}(\text{CN})_4(\text{MeO})_2]^{2-}$, and $\text{trans}-[\{\text{W}_6\text{I}_8\}(\text{CN})_2(\text{MeO})_4]^{2-}$ cluster anions (a–c, respectively). Right: structure of the HOMOs and LUMOs of the $[\{\text{Mo}_6\text{I}_8\}(\text{CN})_6]^{2-}$, $\text{trans}-[\{\text{Mo}_6\text{I}_8\}(\text{CN})_4(\text{MeO})_2]^{2-}$, and $\text{trans}-[\{\text{W}_6\text{I}_8\}(\text{CN})_2(\text{MeO})_4]^{2-}$ cluster anions (a–c, respectively).

2.5. Luminescence Properties

As noted above, 24-electron halide octahedral cluster complexes of molybdenum and tungsten demonstrate bright photoluminescence in the red region with microsecond lifetimes (phosphorescence) [1,3,6,16,37,40,42,52–54]. The spectroscopic and photophysical parameters, namely emission maximum wavelength λ_{em} , lifetimes τ_{em} and quantum yields Φ_{em} for the deaerated acetonitrile solutions of compounds **2**, **4** and **5** as well as for their precursors $(\text{Bu}_4\text{N})_2[\{\text{Mo}_6\text{I}_8\}\text{I}_6]$ and $(\text{Bu}_4\text{N})_2[\{\text{W}_6\text{I}_8\}\text{I}_6]$, are summarized in Table 3. All compounds showed typical broad emission bands with λ_{em} centered around 700 nm (Figure 7). Substitution of iodide apical ligands in $[\{\text{Mo}_6\text{I}_8\}\text{I}_6]^{2-}$ led to a blue-shift of the emission maxima, while transformation of $[\{\text{W}_6\text{I}_8\}\text{I}_6]^{2-}$ into $[\{\text{W}_6\text{I}_8\}(\text{CN})_2(\text{MeO})_4]^{2-}$ resulted in a bathochromic shift of λ_{em} . The emission spectral band shapes of $[\{\text{W}_6\text{I}_8\}(\text{CN})_2(\text{MeO})_4]^{2-}$ is notably broader than the shapes of the $\{\text{Mo}_6\text{I}_8\}^{4+}$ -based complexes (Figure 7). Emission lifetimes of acetonitrile solutions of **2**, **4** and **5** are longer than those of corresponding $[\{\text{M}_6\text{I}_8\}\text{I}_6]^{2-}$ complexes, and τ_{em} values are comparable for hexamolybdenum anions in compounds **2** and **4** and higher than for the hexatungsten complex in **5** (Table 3). The relative emission quantum yields Φ_{em} greatly decrease

in the row $[\text{Mo}_6\text{I}_8(\text{CN})_4(\text{MeO})_2]^{2-} > [\text{Mo}_6\text{I}_8(\text{CN})_6]^{2-} > [\text{W}_6\text{I}_8(\text{CN})_2(\text{MeO})_4]^{2-}$. It is interesting to note that Φ_{em} values of deaerated acetonitrile solutions $[\{\text{Mo}_6\text{I}_8\}(\text{CN})_6]^{2-}$ and $[\{\text{W}_6\text{I}_8\}(\text{CN})_2(\text{MeO})_4]^{2-}$ are very low in comparison with those for the initial cluster complexes. At the same time, Φ_{em} of $[\text{Mo}_6\text{I}_8(\text{CN})_4(\text{MeO})_2]^{2-}$ somewhat exceeds the quantum yield of $[\{\text{Mo}_6\text{I}_8\}\text{I}_6]^{2-}$.

Table 3. Spectroscopic and photophysical parameters of compounds 2, 4 and 5 in deaerated acetonitrile solutions ($\lambda_{\text{ex}} = 360 \text{ nm}$) in comparison with those reported for $(\text{Bu}_4\text{N})_2[\{\text{Mo}_6\text{I}_8\}\text{I}_6]$ and $(\text{Bu}_4\text{N})_2[\{\text{W}_6\text{I}_8\}\text{I}_6]$.

Compound/Anion	Deaerated MeCN Solution		
	$\lambda_{\text{max}}, \text{nm}$	Φ_{em}	$\tau_{\text{em}}, \mu\text{s}$
2/ $[\{\text{Mo}_6\text{I}_8\}(\text{CN})_6]^{2-}$	685	0.02	162
4/ $[\{\text{Mo}_6\text{I}_8\}(\text{CN})_4(\text{MeO})_2]^{2-}$	700	0.14	151
5/ $[\{\text{W}_6\text{I}_8\}(\text{CN})_2(\text{MeO})_4]^{2-}$	720	0.01	92
$(\text{Bu}_4\text{N})_2[\{\text{Mo}_6\text{I}_8\}\text{I}_6]/[\{\text{Mo}_6\text{I}_8\}\text{I}_6]^{2-}$ [54]	730	0.12	90
$(\text{Bu}_4\text{N})_2[\{\text{W}_6\text{I}_8\}\text{I}_6]/[\{\text{W}_6\text{I}_8\}\text{I}_6]^{2-}$ [54]	685	0.23	35

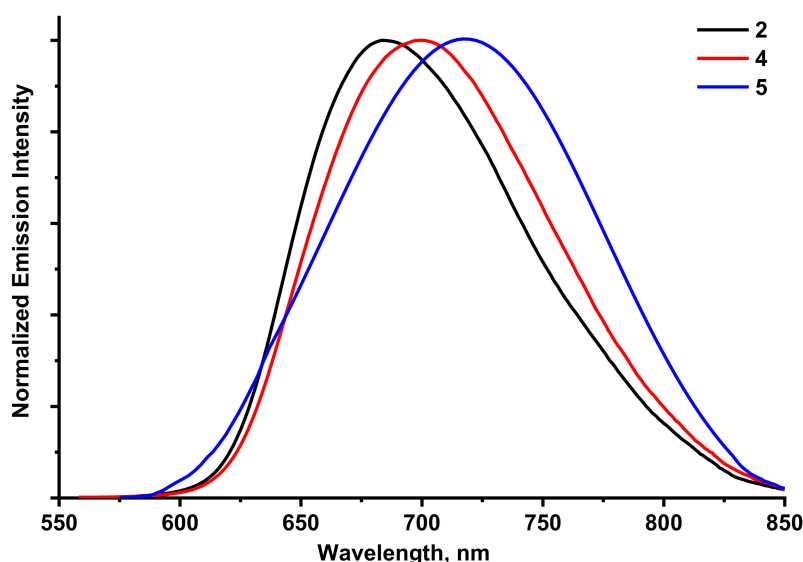


Figure 7. Normalized emission spectra of compounds 2, 4 and 5 in acetonitrile solutions.

3. Materials and Methods

Mo_6I_{12} was synthesized by a high-temperature treatment of stoichiometric amounts of Mo and I_2 at 700°C in a sealed silica tube for 4 days [55]. $(\text{Bu}_4\text{N})_2[\{\text{Mo}_6\text{I}_8\}\text{I}_6]$ was synthesized from $\text{Cs}_2[\{\text{Mo}_6\text{I}_8\}\text{I}_6]$ following the reported procedure [55]. $(\text{Bu}_4\text{N})_2[\{\text{W}_6\text{I}_8\}\text{I}_6]$ was synthesized using the reaction of W_6Cl_{12} with a KI/LiI melt (70/30 mol%) followed by the dissolution of the cooled melt in ethanol and the precipitation of $(\text{Bu}_4\text{N})_2[\{\text{W}_6\text{I}_8\}\text{I}_6]$ by adding Bu_4NI to the solution [56,57]. Other reagents and solvents employed were commercially available and used as received without further purification.

Synthesis of compound 1 was carried out using a vibratory ball mill of the following construction: steel balls with a diameter of 3 mm (total mass 200 g) were charged into a cylindrical steel reactor (100 cm^3 volume and 50 mm height) fitted with a flange cover. The frequency of the vertical reciprocating motion of the reactor was 100 Hz, the amplitude was 10 mm. Elemental (CHN) analysis was performed on a Euro EA3000 CHNS-O Analyzer (EuroVector, Pavia, Lombardy, Italy). Energy-dispersive X-ray spectroscopy (EDS) was performed on TM3000 TableTop Scanning Electron Microscope (Hitachi, Ltd., Marunouchi, Chiyoda-ku, Tokyo, Japan) with QUANTAX 70 EDS for SEM equipment (Bruker Corporation, Billerica, MA, USA). Infrared spectra were recorded with a Vertex 80 FT-IR spectrometer (Bruker Corporation, Billerica, MA, USA) in a KBr pellet. UV-Vis spectra were recorded in H_2O

with a Cary 60 spectrophotometer (Agilent Technologies, Inc., Santa Clara, California, USA) at room temperature in the range 200–600 nm. X-ray powder diffraction data were collected on a PW1820/1710 diffractometer (Philips, Amsterdam, Netherlands) (Cu K α radiation, graphite monochromator, silicon plate used as an external standard). The thermogravimetric properties were studied using a TG 209 F1 Iris Thermo Microbalance (NETZSCH-Gerätebau GmbH, Selb, Germany) in the temperature range of 25–800 °C at a rate of 10°·min⁻¹ in a He flow (30 mL·min⁻¹). The ¹³C-NMR spectra were recorded from a DMSO-d₆ solution at room temperature on Avance III 500 FT-spectrometer (Bruker Corporation, Billerica, MA, USA) with working frequency 125.73 MHz. The ¹³C-NMR chemical shifts are reported in ppm of the δ scale and referred to signals of the solvents (39.50 ppm). Excitation and emission photoluminescence spectra were recorded with a spectrofluorometer Fluorolog 3 spectrofluorometer (Horiba, Ltd., Kyoto, Japan) equipped with ozone-free 450 W Xe lamp, cooled R928/1860 photon detector (Hamamatsu Photonics K.K., Hamamatsu City, Shizuoka, Japan) with refrigerated chamber PC177CE-010 (Products for Research, Inc., Danvers, MA, USA) and double grating monochromators. Excitation and emission spectra were corrected for source intensity and detector spectral response by standard correction curves. The same instrument was used for determination emission lifetimes. The relative emission quantum yields (Φ_{em}) for the deaerated acetonitrile solutions were estimated by using [Ru(bpy)₃]Cl₂ as a standard: $\Phi_{em} = 0.04$ in aerated water [58].

3.1. Synthesis of Cs_{1.3}Na_{0.7}{[Mo₆I₈](CN)₆}·2H₂O (1)

Mo₆I₁₂ (900 mg, 0.43 mmol) and NaCN (700 mg, 14.29 mmol) were placed in the vibratory ball mill. Mechanochemical activation was carried out during 12 h. The reaction products were dissolved in water (100 mL) and filtered forming clear orange solution. Solution of CsCl (200 mg, 1.19 mmol) in 5 mL of H₂O was added, and then the solution was evaporated to a volume of about 10 mL. The forming red crystalline precipitate was filtered off and dried in air. Yield: 615 mg (73%). EDS: Cs:Na:Mo:I = 1.4:0.7:6:8.1. Anal. Calcd. for C₆Cs_{1.3}H₄I₈Mo₆N₆Na_{0.7}O₂: C 3.7, H 0.2, N 4.3. Found C 3.6, H 0.2, N 4.4%. UV-Vis (H₂O): λ_{max} , nm (ϵ , mol⁻¹ dm³ cm⁻¹) 215 (81834), 240 (81897), 272 (25126), 324* (sh, 5407), 391 (4516). IR (cm⁻¹): ν (CN) 2118.

3.2. Synthesis of (Bu₄N)₂{[Mo₆I₈](CN)₆}·0.7H₂O (2)

3.2.1. Metathesis Reaction

Compound 1 (200 mg, 0.10 mmol) was dissolved in 10 mL of H₂O, then a solution of Bu₄NI (100 mg, 0.31 mmol) in 10 mL of H₂O was added. The precipitate was separated by centrifugation, washed with hot water and dried in air. Yield: 180 mg (78%). EDS: Mo:I = 6.0:8.3. Anal. Calcd. for C₃₈H_{73.4}I₈Mo₆N₈O_{0.7}: C 20.3, H 3.3, N 5.0. Found C 20.5, H 3.3, N 5.1%. IR (cm⁻¹): ν (CN) 2121. UV-Vis (CH₃CN): λ_{max} , nm (ϵ , mol⁻¹ dm³ cm⁻¹) 217 (74210), 242 (77041), 273 (22426), 332* (5443), 398 (4572).

3.2.2. Solvothermal Ligand Exchange Reaction

A mixture of (Bu₄N)₂{[Mo₆I₈]I₆} (150 mg, 0.05 mmol) and NaCN (150 mg, 3.06 mmol) were mixed with 3 mL of H₂O in a glass tube. The tube was sealed, heated to 120 °C, held at this temperature for 24 h and then cooled to room temperature at a natural rate (about 50 °C/h). The reaction led to a dark brown insoluble powder and a pale yellow solution. The solution was filtered, evaporated to a volume of about 1 mL, cooled to the room temperature and kept in air. One day later, a few bright red needle crystals of compound 2 precipitated from the solution.

3.3. Synthesis of (Bu₄N)₂{[Mo₆I₈](CN)₆}·2DMSO (3)

Compound 2 (150 mg, 0.076 mmol) was dissolved in 2 mL of DMSO at a temperature of 80 °C. The solution was left at room temperature in a closed vial. Red crystals of compound 3 were precipitated for 12 h. Crystals were collected on a filter paper and dried in air. Yield: 100 mg (63%).

EDS: Mo:I = 6.0:8.3. Anal. Calcd. for $C_{42}H_{84}I_8Mo_6N_8O_2S_2$: C 21.1, H 3.5, N 4.7, S 2.7. Found: C 20.9, H 3.5, N 4.6, S 2.9%. IR (cm^{-1}): $\nu(CN)$ 2115, $\nu(SO)$ 1035.

3.4. Preparation of $(Bu_4N)_2[Mo_6I_8(CN)_4(MeO)_2]$ (4)

A mixture of $(Bu_4N)_2[Mo_6I_8]I_6$ (150 mg, 0.05 mmol) and NaCN (100 mg, 2.04 mmol) were mixed with 5 mL of MeOH in a glass tube. The tube was sealed, heated to 100 °C, held at this temperature for 12 h and then cooled to room temperature at a natural rate (about 50 °C/h). The bright red solution was filtered from excess of NaCN and 5 mL of H_2O were added. The solution was evaporated to about 3 mL, cooled to the room temperature and kept in air. Two days later, dark red block crystals of compound 4 were precipitated. Yield: 102 mg (86%). EDS: Mo:I = 6.0:7.8. Anal. Calcd. for $C_{38}H_{84}I_8Mo_6N_6O_5$: C 19.9, H 3.7, N 3.7. Found: C 20.1, H 3.4, N 3.8%. IR (cm^{-1}): $\nu(CN)$ 2110. UV-Vis (H_2O): λ_{max} , nm (ϵ , $M^{-1} dm^3 cm^{-1}$): 215 (86130), 272 (15060), 382 (3030). ^{13}C -NMR (500 MHz, DMSO- d_6): 14.16, 19.87, 23.72, 58.23 (Bu_4N^+), 39.91 (DMSO- d_6), 69.26 (MeO), 137.19 (CN).

3.5. Preparation of $(Bu_4N)_2[W_6I_8(CN)_2(MeO)_4] \cdot 5H_2O$ (5)

Compound 5 was prepared as described for compound 4 using $(Bu_4N)_2[W_6I_8]I_6$ (150 mg, 0.045 mmol) and NaCN (100 mg, 2.04 mmol) as precursors. The yield of yellow block crystals of 5 was 77 mg (60%). EDS: W:I = 6.0:8.1. Anal. Calcd. for $C_{38}H_{94}I_8N_4O_9W_6$: C 15.9, H 3.3, N 2.0. Found: C 15.9, H 3.3, N 2.1%. IR (cm^{-1}): $\nu(CN)$ 2112. UV-Vis (H_2O): λ , nm (ϵ , $M^{-1} dm^3 cm^{-1}$): 225 (63290), 311 (5890). ^{13}C -NMR (500 MHz, DMSO- d_6): 14.08, 19.83, 23.71, 58.24 (Bu_4N^+), 39.91 (DMSO- d_6), 70.06 (MeO), 137.31 (CN).

3.6. Single Crystal Diffraction Studies

Single crystals of compounds 2–5 were picked up directly from the reaction mixtures. Diffraction data for 2–4 were obtained on an Xcalibur diffractometer (Agilent Technologies, Inc., Santa Clara, California, USA) equipped with an area CCD AtlasS2 detector (Mo $K\alpha$, $\lambda = 0.71073 \text{ \AA}$, graphite monochromator, ω -scans). Integration, absorption correction, and determination of unit cell parameters were performed using the CrysAlisPro program package [59]. Single crystal XRD data for compound 5 were collected with a D8 Venture diffractometer (Bruker Corporation, Billerica, MA, USA) equipped with an area CMOS PHOTON III detector and $I\mu S$ 3.0 source (Mo $K\alpha$, $\lambda = 0.71073 \text{ \AA}$, φ - and ω -scan). Absorption corrections were applied with the use of the SADABS program [60]. All measurements were conducted at 150 K. The structures were solved by a dual space algorithm (SHELXT) [61] and refined by the full-matrix least squares technique (SHELXL) [62] in the anisotropic approximation (except hydrogen atoms). Positions of hydrogen atoms of organic ligands were calculated geometrically and refined in the riding model. Hydrogen atoms of the water molecules were not located. The crystallographic data and details of the structure refinement are summarized in Table 4. Selected bond distances are listed in Table 1. CCDC 2042364–2042367 contain the crystallographic data for 2–5, respectively. These data can be obtained free of charge from The Cambridge Crystallographic Data Centre via www.ccdc.cam.ac.uk/structures.

Table 4. Crystal data, data collection, and refinement parameters for 2–5.

Compound	2	3	4	5
Chemical Formula	(Bu ₄ N) ₂ [Mo ₆ I ₈ (CN) ₆]-0.7H ₂ O	(Bu ₄ N) ₂ [Mo ₆ I ₈ (CN) ₆]-2DMSO	(Bu ₄ N) ₂ [Mo ₆ I ₈ (CN) ₄ (MeO) ₂]	(Bu ₄ N) ₂ [W ₆ I ₈ (MeO) ₄ (CN) ₂]-5H ₂ O
Empirical Formula	C ₃₈ H _{73.4} I ₈ Mo ₆ N ₈ O _{0.7}	C ₄₂ H ₈₄ I ₈ Mo ₆ N ₈ O ₂ S ₂	C ₃₈ H ₇₈ I ₈ Mo ₆ N ₆ O ₂	C ₃₈ H ₉₄ I ₈ N ₄ O ₉ W ₆
Formula Weight	2244.48	2388.13	2241.90	2859.39
Temperature (K)	140(2)	150(2)	150(2)	150(2)
Crystal Size (mm ³)	0.18 × 0.10 × 0.09	0.15 × 0.14 × 0.07	0.16 × 0.15 × 0.08	0.12 × 0.05 × 0.05
Crystal System	Monoclinic	Triclinic	Tetragonal	Monoclinic
Space Group	C2/c	$\bar{P}1$	I4/mmm	P2 ₁ /n
Z	16	1	2	2
a (Å)	37.2726(6)	10.7807(4)	14.6656(3)	9.8189(3)
b (Å)	24.8482(5)	11.4600(5)	14.6656(3)	15.4901(5)
c (Å)	28.2845(5)	15.2964(7)	14.5746(4)	21.8314(8)
α (°)	90	92.784(4)	90	90
β (°)	111.997(2)	91.598(3)	90	97.512(1)
γ (°)	90	113.849(4)	90	90
V (Å ³)	24288.9(8)	1724.1(1)	3134.7(2)	3292.0(2)
D _{calcd.} (g cm ⁻³)	2.455	2.300	2.375	2.895
μ (Mo Kα) (mm ⁻¹)	5.303	4.737	5.137	14.235
θ range (°)	1.95 to 25.35	1.947 to 29.066	1.964 to 29.580	1.882 to 27.482
	-43 ≤ h ≤ 44	-14 ≤ h ≤ 14	-20 ≤ h ≤ 15	-12 ≤ h ≤ 12
<i>h, k, l</i> index ranges	-29 ≤ k ≤ 24	-15 ≤ k ≤ 14	-19 ≤ k ≤ 19	-20 ≤ k ≤ 20
	-34 ≤ l ≤ 22	-20 ≤ l ≤ 11	-14 ≤ l ≤ 19	-25 ≤ l ≤ 28
F(000)	16624	1116	2080	2560
Reflections Collected	57967	12899	8980	50844
Independent Reflections	22209 (R _{int} = 0.0314)	7839 (R _{int} = 0.0177)	1223 (R _{int} = 0.0139)	7549 (R _{int} = 0.0547)
Observed Reflections [I > 2σ(I)]	16412	6675	1101	6533
R Indices [I > 2σ(I)]	R ₁ = 0.0389 wR ₂ = 0.0864	R ₁ = 0.0215 wR ₂ = 0.0457	R ₁ = 0.0199 wR ₂ = 0.0553	R ₁ = 0.0306 wR ₂ = 0.0560
R Indices (all data)	R ₁ = 0.0643 wR ₂ = 0.0952	R ₁ = 0.0289 wR ₂ = 0.0479	R ₁ = 0.0237 wR ₂ = 0.0565	R ₁ = 0.0377 wR ₂ = 0.0591
GOOF on F ²	1.053	0.992	1.091	1.042
Largest Diff. Peak and Hole (e Å ⁻³)	1.745, -1.050	1.305, -0.568	2.815, -0.899	2.042, -1.951

3.7. Computational Details

Density functional theory (DFT) calculations were carried out for $[\{\text{Mo}_6\text{I}_8\}(\text{CN})_6]^{2-}$, $\text{trans}-[\{\text{Mo}_6\text{I}_8\}(\text{CN})_4(\text{MeO})_2]^{2-}$ and $\text{trans}-[\{\text{W}_6\text{I}_8\}(\text{CN})_2(\text{MeO})_4]^{2-}$ clusters in ADF2017 program package (ver. 2017.114, Software for Chemistry & Materials BV, Amsterdam, The Netherlands) [63,64]. Optimization of geometric parameters for the cluster anions in C_1 symmetry was carried out using VWN + S12g dispersion corrected density functional [65–67] and the all-electron TZP basis set [68]. The calculated vibrational spectra contained no imaginary frequencies. Single point calculations of bonding energies and molecular orbitals with geometries from the VWN + S12g/TZP level of theory were carried out with the dispersion-corrected hybrid density functional S12h [67] and the all-electron TZP basis set. The zero-order regular approximation (ZORA) was used in all calculations to take into account the scalar relativistic effects [69]. The calculations were performed using the CH_3CN environment effects, which were added with a Conductor-like Screening Model (COSMO) [70]. The selected calculated interatomic distances are presented in Table 2.

4. Conclusions

In summary, the new octahedral anionic complexes based on $\{\text{Mo}_6\text{I}_8\}^{4+}$ and $\{\text{W}_6\text{I}_8\}^{4+}$ cluster cores with apically homoleptic or heteroleptic coordination environment including ambidentate CN^- ligands were obtained. The $[\{\text{Mo}_6\text{I}_8\}(\text{CN})_6]^{2-}$ cluster anion was synthesized by implementation of mechanochemical activation to the polymeric MoI_2 , while two heteroleptic anionic complexes $\text{trans}-[\{\text{Mo}_6\text{I}_8\}(\text{CN})_4(\text{MeO})_2]^{2-}$ and $\text{trans}-[\{\text{W}_6\text{I}_8\}(\text{CN})_2(\text{MeO})_4]^{2-}$ were synthesized using solvothermal method. Compounds based on the new anions were isolated as crystalline salts in preparative amounts. It was found that the compounds could be recrystallized from aqueous solutions and $\text{H}_2\text{O}/\text{MeOH}$ mixtures, showing excellent hydrolytic stability. Investigation of spectroscopic properties of the new compounds revealed the bright red luminescence with typical lifetimes of the order of 100 microseconds. The relative quantum yield for complex $[\{\text{Mo}_6\text{I}_8\}(\text{CN})_4(\text{MeO})_2]^{2-}$ reached 0.14 in a deoxygenated acetonitrile solution. Note that this is the first report of the luminescence properties of cyanide octahedral clusters of molybdenum and tungsten. Owing to the combination of including ambidentate inert cyanide and labile methylate ligands, the heteroleptic anions can be used as functional building blocks for coordination polymers, as a basis for the directed synthesis of more complex heteroligand clusters, and as promising objects for phototoxicity studies.

Supplementary Materials: The following are available online at. Figure S1: Fragment of structure of the compound 3 with numbered atoms (except hydrogens) of asymmetric unit. Atoms are shown as thermal ellipsoids of 50% probability; Figure S2: Packing of the cluster anions, Bu_4N^+ cations and DMSO molecules in the structure of compound 3, view along a direction. Atoms are shown as thermal ellipsoids of 50% probability; Figure S3: Packing diagram for the compound 4, view along a direction. Atoms are shown as thermal ellipsoids of 50% probability. Hydrogen atoms are not shown. Hydrogen atoms are not shown; Figure S4: Packing diagram for the compound 5, view along a direction. Atoms are shown as thermal ellipsoids of 50% probability. Hydrogen atoms are not shown.

Author Contributions: Realization of the experiments and analysis of the experimental data, A.S.P. and S.S.Y.; calculation of the electronic structures, Y.M.G.; investigation of luminescence properties, A.A.R. and K.A.B.; investigation of crystal structures, D.G.S.; NMR experiments, I.V.E.; draft preparation, A.S.P. and Y.M.G.; manuscript editing, Y.M.G. and K.A.B.; conceptualization and supervision, Y.V.M. All authors have read and agreed to the published version of the manuscript.

Funding: This work was financially supported by Russian Foundation for Basic Research (project 18-29-04007). Luminescence measurements were supported by the grant of Russian Science Foundation (project 19-73-20196). Measurements were performed in “Center for Optical and Laser materials research” (St. Petersburg State University, St. Petersburg, Russian Federation).

Acknowledgments: The authors thank V.Y. Komarov (XRD Centre of NIIC SB RAS) for providing the single crystal XRD data collection.

Conflicts of Interest: The authors declare no conflict of interest.

References

1. Sokolov, M.N.; Brylev, K.A.; Abramov, P.A.; Gallyamov, M.R.; Novozhilov, I.N.; Kitamura, N.; Mikhaylov, M.A. Complexes of $\{W_6I_8\}^{4+}$ Clusters with Carboxylates: Preparation, Electrochemistry, and Luminescence. *Eur. J. Inorg. Chem.* **2017**, *2017*, 4131–4137. [[CrossRef](#)]
2. Seyboldt, A.; Enseling, D.; Jüstel, T.; Ivanović, M.; Peisert, H.; Chassé, T.; Meyer, H.-J. Ligand Influence on the Photophysical Properties and Electronic Structures of Tungsten Iodide Clusters. *Eur. J. Inorg. Chem.* **2017**, *2017*, 5387–5394. [[CrossRef](#)]
3. Kirakci, K.; Fejfarová, K.; Kučeráková, M.; Lang, K. Hexamolybdenum Cluster Complexes with Pyrene and Anthracene Carboxylates: Ultrabright Red Emitters with the Antenna Effect. *Eur. J. Inorg. Chem.* **2014**, *2014*, 2331–2336. [[CrossRef](#)]
4. Zietlow, T.C.; Nocera, D.G.; Gray, H.B. Photophysics and Electrochemistry of Hexanuclear Tungsten Halide Clusters. *Inorg. Chem.* **1986**, *25*, 1351–1353. [[CrossRef](#)]
5. Maverick, A.W.; Najdzionek, J.S.; MacKenzie, D.; Nocera, D.G.; Gray, H.B. Spectroscopic, Electrochemical, and Photochemical Properties of Molybdenum(II) and Tungsten(II) Halide Clusters. *J. Am. Chem. Soc.* **1983**, *105*, 1878–1882. [[CrossRef](#)]
6. Akagi, S.; Fujii, S.; Kitamura, N. A study on the redox, spectroscopic, and photophysical characteristics of a series of octahedral hexamolybdenum(ii) clusters: $[\{Mo_6X_8\}Y_6]^{2-}$ (X, Y = Cl, Br, or I). *Dalton Trans.* **2018**, *47*, 1131–1139. [[CrossRef](#)]
7. Mikhaylov, M.A.; Sokolov, M.N. Molybdenum Iodides – from Obscurity to Bright Luminescence. *Eur. J. Inorg. Chem.* **2019**, *2019*, 4181–4197. [[CrossRef](#)]
8. Fujii, S.; Horiguchi, T.; Akagi, S.; Kitamura, N. Quasi-One-Step Six-Electron Electrochemical Reduction of an Octahedral Hexanuclear Molybdenum(II) Cluster. *Inorg. Chem.* **2016**, *55*, 10259–10266. [[CrossRef](#)]
9. Cordier, S.; Fabre, B.; Molard, Y.; Fadje-Djomkam, A.-B.; Turban, P.; Tricot, S.; Ababou-Girard, S.; Godet, C. Elaboration, Characterizations, and Energetics of Robust Mo_6 Cluster-Terminated Silicon-Bound Molecular Junctions. *J. Phys. Chem. C* **2016**, *120*, 2324–2334. [[CrossRef](#)]
10. Barras, A.; Das, M.R.; Devarapalli, R.R.; Shelke, M.V.; Cordier, S.; Szunerits, S.; Boukherroub, R. One-pot synthesis of gold nanoparticle/molybdenum cluster/graphene oxide nanocomposite and its photocatalytic activity. *Appl. Catal. B Environ.* **2013**, *130–131*, 270–276. [[CrossRef](#)]
11. Feliz, M.; Puche, M.; Atienzar, P.; Concepción, P.; Cordier, S.; Molard, Y. In Situ Generation of Active Molybdenum Octahedral Clusters for Photocatalytic Hydrogen Production from Water. *ChemSusChem* **2016**, *9*, 1963–1971. [[CrossRef](#)] [[PubMed](#)]
12. Kumar, P.; Mungse, H.P.; Cordier, S.; Boukherroub, R.; Khatri, O.P.; Jain, S.L. Hexamolybdenum clusters supported on graphene oxide: Visible-light induced photocatalytic reduction of carbon dioxide into methanol. *Carbon* **2015**, *94*, 91–100. [[CrossRef](#)]
13. Feliz, M.; Atienzar, P.; Amela-Cortés, M.; Dumait, N.; Lemoine, P.; Molard, Y.; Cordier, S. Supramolecular Anchoring of Octahedral Molybdenum Clusters onto Graphene and Their Synergies in Photocatalytic Water Reduction. *Inorg. Chem.* **2019**, *58*, 15443–15454. [[CrossRef](#)] [[PubMed](#)]
14. Cîrcu, V.; Molard, Y.; Amela-Cortés, M.; Bentaleb, A.; Barois, P.; Dorcet, V.; Cordier, S. From Mesomorphic Phosphine Oxide to Clustomesogens Containing Molybdenum and Tungsten Octahedral Cluster Cores. *Angew. Chem. Int. Ed.* **2015**, *54*, 10921–10925. [[CrossRef](#)] [[PubMed](#)]
15. Efremova, O.A.; Shestopalov, M.A.; Chirtsova, N.A.; Smolentsev, A.I.; Mironov, Y.V.; Kitamura, N.; Brylev, K.A.; Sutherland, A.J. A highly emissive inorganic hexamolybdenum cluster complex as a handy precursor for the preparation of new luminescent materials. *Dalton Trans.* **2014**, *43*, 6021–6025. [[CrossRef](#)]
16. Kirakci, K.; Kubát, P.; Langmaier, J.; Polívka, T.; Fuciman, M.; Fejfarová, K.; Lang, K. A comparative study of the redox and excited state properties of $(nBu_4N)_2[Mo_6X_{14}]$ and $(nBu_4N)_2[Mo_6X_8(CF_3COO)_6]$ (X = Cl, Br, or I). *Dalton Trans.* **2013**, *42*, 7224–7232. [[CrossRef](#)]
17. Jackson, J.A.; Turro, C.; Newsham, M.D.; Nocera, D.G. Oxygen quenching of electronically excited hexanuclear molybdenum and tungsten halide clusters. *J. Phys. Chem.* **1990**, *94*, 4500–4507. [[CrossRef](#)]
18. Solovieva, A.O.; Vorotnikov, Y.A.; Trifonova, K.E.; Efremova, O.A.; Krasilnikova, A.A.; Brylev, K.A.; Vorontsova, E.V.; Avrorov, P.A.; Shestopalova, L.V.; Poveschenko, A.F.; et al. Cellular internalisation, bioimaging and dark and photodynamic cytotoxicity of silica nanoparticles doped by $\{Mo_6I_8\}^{4+}$ metal clusters. *J. Mater. Chem. B* **2016**, *4*, 4839–4846. [[CrossRef](#)]

19. Svezhentseva, E.V.; Solovieva, A.O.; Vorotnikov, Y.A.; Kurskaya, O.G.; Brylev, K.A.; Tsygankova, A.R.; Edeleva, M.V.; Gyrylova, S.N.; Kitamura, N.; Efremova, O.A.; et al. Water-soluble hybrid materials based on $\{Mo_6X_8\}^{4+}$ (X = Cl, Br, I) cluster complexes and sodium polystyrene sulfonate. *New J. Chem.* **2017**, *41*, 1670–1676. [[CrossRef](#)]
20. Brandhonneur, N.; Hatahet, T.; Amela-Cortes, M.; Molard, Y.; Cordier, S.; Dollo, G. Molybdenum cluster loaded PLGA nanoparticles: An innovative theranostic approach for the treatment of ovarian cancer. *Eur. J. Pharm. Biopharm.* **2018**, *125*, 95–105. [[CrossRef](#)]
21. Cheplakova, A.M.; Solovieva, A.O.; Pozmogova, T.N.; Vorotnikov, Y.A.; Brylev, K.A.; Vorotnikova, N.A.; Vorontsova, E.V.; Mironov, Y.V.; Poveshchenko, A.F.; Kovalenko, K.A.; et al. Nanosized mesoporous metal–organic framework MIL-101 as a nanocarrier for photoactive hexamolybdenum cluster compounds. *J. Inorg. Biochem.* **2017**, *166*, 100–107. [[CrossRef](#)] [[PubMed](#)]
22. Elistratova, J.; Mukhametshina, A.; Kholin, K.; Nizameev, I.; Mikhailov, M.; Sokolov, M.; Khairullin, R.; Miftakhova, R.; Shammass, G.; Kadirov, M.; et al. Interfacial uploading of luminescent hexamolybdenum cluster units onto amino-decorated silica nanoparticles as new design of nanomaterial for cellular imaging and photodynamic therapy. *J. Colloid Interf. Sci.* **2019**, *538*, 387–396. [[CrossRef](#)] [[PubMed](#)]
23. Beltrán, A.; Mikhailov, M.; Sokolov, M.N.; Pérez-Laguna, V.; Rezusta, A.; Revillo, M.J.; Galindo, F. A photobleaching resistant polymer supported hexanuclear molybdenum iodide cluster for photocatalytic oxygenations and photodynamic inactivation of *Staphylococcus aureus*. *J. Mater. Chem. B* **2016**, *4*, 5975–5979. [[CrossRef](#)] [[PubMed](#)]
24. Felip-León, C.; Arnau del Valle, C.; Pérez-Laguna, V.; Isabel Millán-Lou, M.; Miravet, J.F.; Mikhailov, M.; Sokolov, M.N.; Rezusta-López, A.; Galindo, F. Superior performance of macroporous over gel type polystyrene as a support for the development of photo-bactericidal materials. *J. Mater. Chem. B* **2017**, *5*, 6058–6064. [[CrossRef](#)] [[PubMed](#)]
25. Rojas-Mancilla, E.; Oyarce, A.; Verdugo, V.; Morales-Verdejo, C.; Echeverría, C.; Velásquez, F.; Chnaiderman, J.; Valiente-Echeverría, F.; Ramirez-Tagle, R. The $[Mo_6Cl_{14}]^{2-}$ Cluster is Biologically Secure and Has Anti-Rotavirus Activity In Vitro. *Molecules* **2017**, *22*, 1108. [[CrossRef](#)] [[PubMed](#)]
26. Neaime, C.; Amela-Cortes, M.; Grasset, F.; Molard, Y.; Cordier, S.; Dierre, B.; Mortier, M.; Takei, T.; Takahashi, K.; Haneda, H.; et al. Time-gated luminescence bioimaging with new luminescent nanocolloids based on $[Mo_6I_8(C_2F_5COO)_6]^{2-}$ metal atom clusters. *Phys. Chem. Chem. Phys.* **2016**, *18*, 30166–30173. [[CrossRef](#)] [[PubMed](#)]
27. Vorotnikova, N.A.; Edeleva, M.V.; Kurskaya, O.G.; Brylev, K.A.; Shestopalov, A.M.; Mironov, Y.V.; Sutherland, A.J.; Efremova, O.A.; Shestopalov, M.A. One-pot synthesis of $\{Mo_6I_8\}^{4+}$ -doped polystyrene microspheres via a free radical dispersion copolymerisation reaction. *Polym. Int.* **2017**, *66*, 1906–1912. [[CrossRef](#)]
28. Fedorov, V.E.; Naumov, N.G.; Mironov, Y.V.; Virovets, A.V.; Artemkina, S.B.; Brylev, K.A.; Yarovoi, S.S.; Efremova, O.A.; Peak, U.H. Inorganic Coordination Polymers Based on Chalcocyanide Cluster Complexes. *J. Struct. Chem.* **2002**, *43*, 669–684. [[CrossRef](#)]
29. Alexandrov, E.V.; Virovets, A.V.; Blatov, V.A.; Peresyphkina, E.V. Topological Motifs in Cyanometallates: From Building Units to Three-Periodic Frameworks. *Chem. Rev.* **2015**, *115*, 12286–12319. [[CrossRef](#)]
30. Efremova, O.A.; Mironov, Y.V.; Fedorov, V.E. Design of Cyano-Bridged Coordination Polymers Based on Tetrahedral Rhenium Cluster Cyanide Complexes and 3d Transition Metals. *Eur. J. Inorg. Chem.* **2006**, *2006*, 2533–2549. [[CrossRef](#)]
31. Amela-Cortes, M.; Cordier, S.; Naumov, N.G.; Mériadec, C.; Artzner, F.; Molard, Y. Hexacyano octahedral metallic clusters as versatile building blocks in the design of extended polymeric framework and clustomesogens. *J. Mater. Chem. C* **2014**, *2*, 9813–9823. [[CrossRef](#)]
32. Daigne, G.; Lemoine, P.; Pham, T.D.; Demange, V.; Gautier, R.; Naumov, N.G.; Ledneva, A.; Amela-Cortes, M.; Dumait, N.; Audebrand, N.; et al. Low dimensional solids based on Mo_6 cluster cyanides and Mn^{2+} , Mn^{3+} or Cd^{2+} metal ions: Crystal chemistry, magnetic and optical properties. *CrystEngComm* **2018**, *20*, 3396–3408. [[CrossRef](#)]
33. Fedin, V.P.; Sokolov, M.N.; Myakishev, K.G.; Geras'ko, O.A.; Fedorov, V.Y.; Maciček, J. Mechanochemical synthesis of soluble complexes containing $M_3S_7^{4+}$ and $M_3Se_7^{4+}$ fragments from polymeric $M_3Y_7Br_4$ (M. = Mo, W; Y = S, Se). The crystal structure of $(PPN)_2W_3S_7Cl_6$. *Polyhedron* **1991**, *10*, 1311–1317. [[CrossRef](#)]

34. Szczepura, L.F.; Ketcham, K.A.; Ooro, B.A.; Edwards, J.A.; Templeton, J.N.; Cedeño, D.L.; Jircitano, A.J. Synthesis and Study of Hexanuclear Molybdenum Clusters Containing Thiolate Ligands. *Inorg. Chem.* **2008**, *47*, 7271–7278. [[CrossRef](#)] [[PubMed](#)]
35. Kirakci, K.; Kubát, P.; Kučeráková, M.; Šícha, V.; Gbelcová, H.; Lovecká, P.; Grznárová, P.; Ruml, T.; Lang, K. Water-soluble octahedral molybdenum cluster compounds $\text{Na}_2[\text{Mo}_6\text{I}_8(\text{N}_3)_6]$ and $\text{Na}_2[\text{Mo}_6\text{I}_8(\text{NCS})_6]$: Syntheses, luminescence, and in vitro studies. *Inorg. Chim. Acta* **2016**, *441*, 42–49. [[CrossRef](#)]
36. Vorotnikov, Y.A.; Efremova, O.A.; Novozhilov, I.N.; Yanshole, V.V.; Kuratieva, N.V.; Brylev, K.A.; Kitamura, N.; Mironov, Y.V.; Shestopalov, M.A. Hexaazide octahedral molybdenum cluster complexes: Synthesis, properties and the evidence of hydrolysis. *J. Mol. Struct.* **2017**, *1134*, 237–243. [[CrossRef](#)]
37. Kirakci, K.; Demel, J.; Hynek, J.; Zelenka, J.; Rumlová, M.; Ruml, T.; Lang, K. Phosphinate Apical Ligands: A Route to a Water-Stable Octahedral Molybdenum Cluster Complex. *Inorg. Chem.* **2019**, *58*, 16546–16552. [[CrossRef](#)] [[PubMed](#)]
38. Svezhentseva, E.V.; Vorotnikov, Y.A.; Solovieva, A.O.; Pozmogova, T.N.; Eltsov, I.V.; Ivanov, A.A.; Evtushok, D.V.; Miroschnichenko, S.M.; Yanshole, V.V.; Eling, C.J.; et al. From Photoinduced to Dark Cytotoxicity through an Octahedral Cluster Hydrolysis. *Chem. Eur. J.* **2018**, *24*, 17915–17920. [[CrossRef](#)] [[PubMed](#)]
39. Aubert, T.; Burel, A.; Esnault, M.-A.; Cordier, S.; Grasset, F.; Cabello-Hurtado, F. Root uptake and phytotoxicity of nanosized molybdenum octahedral clusters. *J. Hazard. Mater.* **2012**, *219–220*, 111–118. [[CrossRef](#)] [[PubMed](#)]
40. Efremova, O.A.; Vorotnikov, Y.A.; Brylev, K.A.; Vorotnikova, N.A.; Novozhilov, I.N.; Kuratieva, N.V.; Edeleva, M.V.; Benoit, D.M.; Kitamura, N.; Mironov, Y.V.; et al. Octahedral molybdenum cluster complexes with aromatic sulfonate ligands. *Dalton Trans.* **2016**, *45*, 15427–15435. [[CrossRef](#)] [[PubMed](#)]
41. Brückner, P.; Preetz, W.; Pünjer, M. Darstellung, Kristallstrukturen, NMR-, Schwingungsspektren und Normalkoordinatenanalyse der Clusteranionen $[(\text{Mo}_6\text{I})\text{Y}]^{2-}$, $\text{Ya} = \text{F}, \text{Cl}, \text{Br}$, I.Z. *Anorg. Allg. Chem.* **1997**, *623*, 8–17. [[CrossRef](#)]
42. Mikhailov, M.A.; Brylev, K.A.; Abramov, P.A.; Sakuda, E.; Akagi, S.; Ito, A.; Kitamura, N.; Sokolov, M.N. Synthetic Tuning of Redox, Spectroscopic, and Photophysical Properties of $[\text{Mo}_6\text{I}_8]^{4+}$ Core Cluster Complexes by Terminal Carboxylate Ligands. *Inorg. Chem.* **2016**, *55*, 8437–8445. [[CrossRef](#)] [[PubMed](#)]
43. Simsek, M.K.; Bublitz, D.; Preetz, W. Darstellung, Kristallstrukturen, Schwingungsspektren und Normalkoordinatenanalyse von $[(\text{Mo}_6\text{Br})\text{Y}]^{2-}$; $\text{Ya} = \text{CN}, \text{NCS}$. *Z. Anorg. Allg. Chem.* **1997**, *623*, 1885–1891. [[CrossRef](#)]
44. Cordier, S.; Naumov, N.G.; Salloum, D.; Paul, F.; Perrin, C. Synthesis and Characterization of Mo_6 Chalcobromides and Cyano-Substituted Compounds Built from a Novel $[(\text{Mo}_6\text{Br}^i\text{Y}^i_2)\text{L}^a_6]^{n-}$ Discrete Cluster Unit ($\text{Y}^i = \text{S}$ or Se and $\text{L}^a = \text{Br}$ or CN). *Inorg. Chem.* **2004**, *43*, 219–226. [[CrossRef](#)]
45. Petunin, A.A.; Evtushok, D.V.; Vorotnikova, N.A.; Kuratieva, N.V.; Vorotnikov, Y.A.; Shestopalov, M.A. Hexasubstituted Iodide Tungsten Cluster Complexes with Azide and Isothiocyanate Ligands. *Eur. J. Inorg. Chem.* **2020**, *2020*, 2177–2181. [[CrossRef](#)]
46. Riehl, L.; Seyboldt, A.; Ströbele, M.; Enseling, D.; Jüstel, T.; Westberg, M.; Ogilby, P.R.; Meyer, H.J. A ligand substituted tungsten iodide cluster: Luminescence vs. singlet oxygen production. *Dalton Trans.* **2016**, *45*, 15500–15506. [[CrossRef](#)]
47. Mikhailov, M.A.; Abramov, P.A.; Mironova, A.D.; Gallyamov, M.R.; Sheven', D.G.; Pervukhin, V.V.; Sokolov, M.N. Methyl Propiolate Cluster Complex $(\text{Ph}_4\text{P})_2[\text{W}_6\text{I}_8(\text{C}\equiv\text{C}-\text{C}(\text{O})\text{OCH}_3)_6]$. *Russ. J. Coord. Chem.* **2019**, *45*, 56–61. [[CrossRef](#)]
48. Costuas, K.; Garreau, A.; Bulou, A.; Fontaine, B.; Cuny, J.; Gautier, R.; Mortier, M.; Molard, Y.; Duvail, J.L.; Faulques, E.; et al. Combined theoretical and time-resolved photoluminescence investigations of $[\text{Mo}_6\text{Br}^i_8\text{Br}^a_6]^{2-}$ metal cluster units: Evidence of dual emission. *Phys. Chem. Chem. Phys.* **2015**, *17*, 28574–28585. [[CrossRef](#)]
49. Gray, T.G. Divergent Electronic Structures of Isoelectronic Metalloclusters: Tungsten(II) Halides and Rhenium(III) Chalcogenide Halides. *Chem. Eur. J.* **2009**, *15*, 2581–2593. [[CrossRef](#)]
50. Ramirez-Tagle, R.; Arratia-Pérez, R. Electronic structure and molecular properties of the $[\text{Mo}_6\text{X}_8\text{L}_6]^{2-}$; $\text{X} = \text{Cl}, \text{Br}, \text{I}$; $\text{L} = \text{F}, \text{Cl}, \text{Br}, \text{I}$ clusters. *Chem. Phys. Lett.* **2008**, *460*, 438–441. [[CrossRef](#)]
51. Robinson, L.M.; Bain, R.L.; Shriver, D.F.; Ellis, D.E. Effect of Coordination Environment on the Electronic Structure and Properties of Mo_6 -Based Systems: A Density Functional Treatment. *Inorg. Chem.* **1995**, *34*, 5588–5596. [[CrossRef](#)]

52. Sokolov, M.N.; Mihailov, M.A.; Peresyphkina, E.V.; Brylev, K.A.; Kitamura, N.; Fedin, V.P. Highly luminescent complexes $[\text{Mo}_6\text{X}_8(\text{n-C}_3\text{F}_7\text{COO})_6]^{2-}$ (X = Br, I). *Dalton Trans.* **2011**, *40*, 6375–6377. [[CrossRef](#)] [[PubMed](#)]
53. Sokolov, M.N.; Mikhailov, M.A.; Brylev, K.A.; Virovets, A.V.; Vicent, C.; Kompankov, N.B.; Kitamura, N.; Fedin, V.P. Alkynyl complexes of high-valence clusters. Synthesis and luminescence properties of $[\text{Mo}_6\text{I}_8(\text{C}\equiv\text{CC}(\text{O})\text{OMe})_6]^{2-}$, the first complex with exclusively organometallic outer ligands in the family of octahedral $\{\text{M}_6\text{X}_8\}$ clusters. *Inorg. Chem.* **2013**, *52*, 12477–12481. [[CrossRef](#)] [[PubMed](#)]
54. Evtushok, D.V.; Melnikov, A.R.; Vorotnikova, N.A.; Vorotnikov, Y.A.; Ryadun, A.A.; Kuratieva, N.V.; Kozyr, K.V.; Obedinskaya, N.R.; Kretov, E.I.; Novozhilov, I.N.; et al. A comparative study of optical properties and X-ray induced luminescence of octahedral molybdenum and tungsten cluster complexes. *Dalton Trans.* **2017**, *46*, 11738–11747. [[CrossRef](#)] [[PubMed](#)]
55. Kirakci, K.; Cordier, S.; Perrin, C. Synthesis and Characterization of $\text{Cs}_2\text{Mo}_6\text{X}_{14}$ (X = Br or I) Hexamolybdenum Cluster Halides: Efficient Mo_6 Cluster Precursors for Solution Chemistry Syntheses. *Z. Anorg. Allg. Chem.* **2005**, *631*, 411–416. [[CrossRef](#)]
56. Vorotnikov, Y.A.; Mikhailov, M.A.; Brylev, K.A.; Piryazev, D.A.; Kuratieva, N.V.; Sokolov, M.N.; Mironov, Y.V.; Shestopalov, M.A. Synthesis, crystal structure, and luminescence properties of complexes $(4\text{-ViBnNMe}_3)_2[\text{M}_6(\mu_3\text{-I})_8]\text{I}_6$ (M = Mo, W; $(4\text{-ViBnNMe}_3)^+$ is trimethyl(4-vinylbenzyl)ammonium). *Russ. Chem. Bull.* **2015**, *64*, 2591–2596. [[CrossRef](#)]
57. Hogue, R.D.; McCarley, R.E. Chemistry of polynuclear metal halides. V. Reactions and characterization of compounds containing tungsten halide cluster species. *Inorg. Chem.* **1970**, *9*, 1354–1360. [[CrossRef](#)]
58. Ishida, H.; Tobita, S.; Hasegawa, Y.; Katoh, R.; Nozaki, K. Recent advances in instrumentation for absolute emission quantum yield measurements. *Coord. Chem. Rev.* **2010**, *254*, 2449–2458. [[CrossRef](#)]
59. *CrysAlisPro 1.171.39.46*; Rigaku Oxford Diffraction: The Woodlands, TX, USA, 2018.
60. APEX3; SAINT; SADABS. *Bruker Advanced X-ray Solutions*; Bruker AXS Inc.: Madison, WI, USA, 2016.
61. Sheldrick, G. SHELXT-Integrated space-group and crystal-structure determination. *Acta Cryst. A* **2015**, *71*, 3–8. [[CrossRef](#)]
62. Sheldrick, G. Crystal structure refinement with SHELXL. *Acta Cryst. C* **2015**, *71*, 3–8. [[CrossRef](#)]
63. Te Velde, G.; Bickelhaupt, F.M.; Baerends, E.J.; Fonseca Guerra, C.; van Gisbergen, S.J.A.; Snijders, J.G.; Ziegler, T. Chemistry with ADF. *J. Comput. Chem.* **2001**, *22*, 931–967. [[CrossRef](#)]
64. Fonseca Guerra, C.; Snijders, J.G.; te Velde, G.; Baerends, E.J. Towards an order-N DFT method. *Theor. Chem. Acc.* **1998**, *99*, 391–403. [[CrossRef](#)]
65. Vosko, S.H.; Wilk, L.; Nusair, M. Accurate spin-dependent electron liquid correlation energies for local spin density calculations: A critical analysis. *Can. J. Phys.* **1980**, *58*, 1200–1211. [[CrossRef](#)]
66. Perdew, J.P.; Wang, Y. Accurate and simple analytic representation of the electron-gas correlation energy. *Phys. Rev. B* **1992**, *45*, 13244–13249. [[CrossRef](#)] [[PubMed](#)]
67. Swart, M. A new family of hybrid density functionals. *Chem. Phys. Lett.* **2013**, *580*, 166–171. [[CrossRef](#)]
68. Van Lenthe, E.; Baerends, E.J. Optimized Slater-type basis sets for the elements 1–118. *J. Comput. Chem.* **2003**, *24*, 1142–1156. [[CrossRef](#)]
69. van Lenthe, E.; Ehlers, A.; Baerends, E.-J. Geometry optimizations in the zero order regular approximation for relativistic effects. *J. Chem. Phys.* **1999**, *110*, 8943–8953. [[CrossRef](#)]
70. Pye, C.C.; Ziegler, T. An implementation of the conductor-like screening model of solvation within the Amsterdam density functional package. *Theor. Chem. Acc.* **1999**, *101*, 396–408. [[CrossRef](#)]

Sample Availability: Samples of compounds 1–5 are available from the authors.

Publisher’s Note: MDPI stays neutral with regard to jurisdictional claims in published maps and institutional affiliations.



© 2020 by the authors. Licensee MDPI, Basel, Switzerland. This article is an open access article distributed under the terms and conditions of the Creative Commons Attribution (CC BY) license (<http://creativecommons.org/licenses/by/4.0/>).